Journal of Nuclear Materials 103 & 104 (1981) 327-332
North-Holland Publishing Company

FIRST WALL EVAPORATION IN INERTIAL CONFINEMENT FUSION REACTORS UTILIZING GAS PROTECTION

A.M. Hassanein, T.J. McCarville, and G.L. Kulcinski

Fusion Engineering Program, Nuclear Engineering Department
University of Wisconsin, Madison, WI 53706, USA

The evaporation of inertial confinement fusion first wall materials from unattenuated pellet X-rays and from radiation emitted by a cavity buffer gas is examined. The low vapor pressure and low X-ray attenuation coefficient of carbon give it a lower erosion rate than stainless steel, despite the larger thermal conductivity of Type 316 stainless steel. For the argon buffer gas containing 0.2% Na and pellet yield used in this study, a gas density greater than 0.3 torr (0°C) is required to prevent evaporative erosion of a carbon first wall. A gas density greater than 0.9 torr (0°C) is needed to prevent erosion of a stainless steel wall.

1. INTRODUCTION

One of the difficulties of designing inertial confinement fusion (ICF) reactors for commercial use is to construct a cavity first wall capable of withstanding the pulsed thermal loads that result from the fusion process. The different types of radiation released by an ICF target explosion are shown schematically in Figure 1. The 10 to 14 MeV neutrons have a large mean free path compared to the first wall thickness, and will pass through without depositing a significant amount of energy. In contrast to the neutrons, the target X-ray and debris energy will be absorbed in the first few microns of an unprotected first wall. If the lifetime of a commercial ICF reactor first wall is to be on the order of 20 full power years, the erosion rate must not exceed a few angstroms per shot. However, previous studies [1] have shown that the evaporation of an unprotected first wall will be a few microns per shot due to the target X-rays and debris.

One method of prolonging the first wall lifetime is to fill the cavity with a buffer gas [2]. The target explosion, gas response, and first wall response are depicted schematically in Figure 1. The X-ray and debris energy of the target is attenuated by the gas, which reradiates the absorbed energy to the first wall. Even if the debris is completely attenuated by the gas, unattenuated target X-rays and gas reradiation may still cause significant evaporation. One objective of this paper is to identify characteristics of the unattenuated X-ray and gas reradiation that lead to excessive evaporation. To meet this objective, the evaporation of both carbon and stainless steel has been computed for various X-ray spectra and gas reradiation characteristics.

The different types of drivers being considered for ICF reactors have widely varying restrictions on the allowable cavity gas density. Hence, the second objective of this paper is to

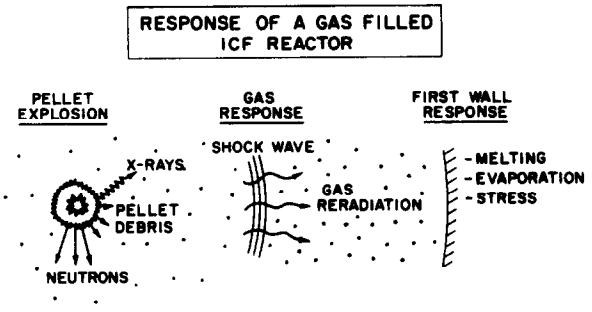

Figure 1. Cavity phenomena in gas filled ICF reactors.

investigate the first wall evaporation from unattenuated X-rays and gas reradiation as a function of the buffer gas density. To meet the second objective, a particular reactor geometry, target X-ray and debris spectra, and buffer gas have been selected. The evaporation of a carbon and a stainless steel first wall is compared for gas densities corresponding to 0.05, 0.5, and 5.0 torr (0°C) and the ambient temperature is assumed to be 573°K.

2. FIRST WALL EVAPORATION FROM GAS RERADIATION AND UNATTENUATED X-RAYS

The first wall thermal response and evaporation calculations that are presented in this paper were computed with the A*THERMAL computer code [3]. The code solves the heat conduction equation with temperature varying thermal properties, and uses the surface temperature to compute the evaporation rate. Moving boundary

conditions are used to account for surface recession from evaporation and also for the solid-liquid interface. For a description of the solution methods and a review of the evaporation models see ref. [4]. The thermal properties of Type 316 stainless steel and Type 3474 D graphite used in this study are given in refs. [5,6].

The general characteristics of first wall evaporation from unattenuated target X-rays can be identified without specifying a particular target design or buffer gas. Figure 2 shows the evaporated thickness of carbon and stainless steel as a function of the X-ray energy spectrum and energy fluence. In Figure 2, it is assumed that the X-ray pulse is 10 nanoseconds long, and that the energy spectrum absorbed by the wall has a blackbody distribution. An exponential energy deposition profile for X-rays is assumed. It is based on the analytical approximations for the absorption cross sections given by Biggs [7]. Figure 2 shows how strongly the evaporated thickness depends on the energy spectrum of the X-rays. To relate cavity dimensions to energy fluence, note that for a spherical cavity 4 meters in radius, 1 J/cm^2 corresponds to about 2 MJ of energy. The X-ray absorption cross sections are such that X-ray penetration into the first wall decreases as the blackbody temperature of the spectrum decreases. As implied in Figure 2, a reduction in penetration depth leads to a larger specific energy density, and consequently to greater evaporation. Hence, even 1 J/cm^2 of X-ray energy with a 0.1 keV blackbody distribution will limit the life of a stainless steel first wall to less than the life of a commercial plant. If there is a gas in the cavity, the softer part of the X-ray spectrum tends to be absorbed by the gas, thereby reducing the evaporation significantly.

There are a number of reasons why a given spectrum of X-rays evaporates less carbon than stainless steel. The primary reason is that the lower atomic number of carbon leads to a lower X-ray absorption cross section, and consequently to a lower specific energy density. Also, at a given temperature carbon also has a lower vapor pressure than stainless steel. For absorbing ICF X-ray pulses, the advantage of carbon is only slightly compromised by its low thermal conductivity.

First wall evaporation from gas reradiation can also be studied without specifying the details of the target spectra, reactor geometry, or reradiation properties of the gas. Figure 3 shows the evaporation of carbon and stainless steel for various reradiation pulse times and energy fluences. In Figure 3, the reradiation heat flux was assumed to be constant over the reradiation time. It was also assumed that the photons reradiated by the gas have a small enough penetration depth into the wall that a surface heat flux model can be used in solving the temperature equation.

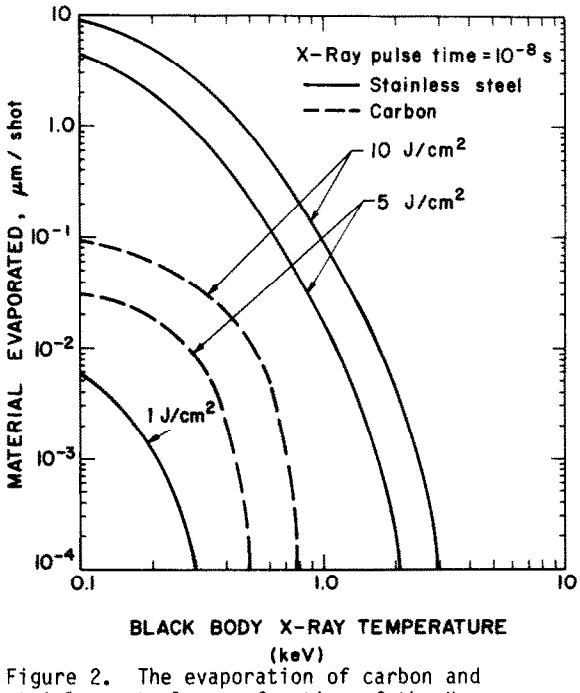

Figure 2. The evaporation of carbon and stainless steel as a function of the X-ray spectrum and the energy fluence.

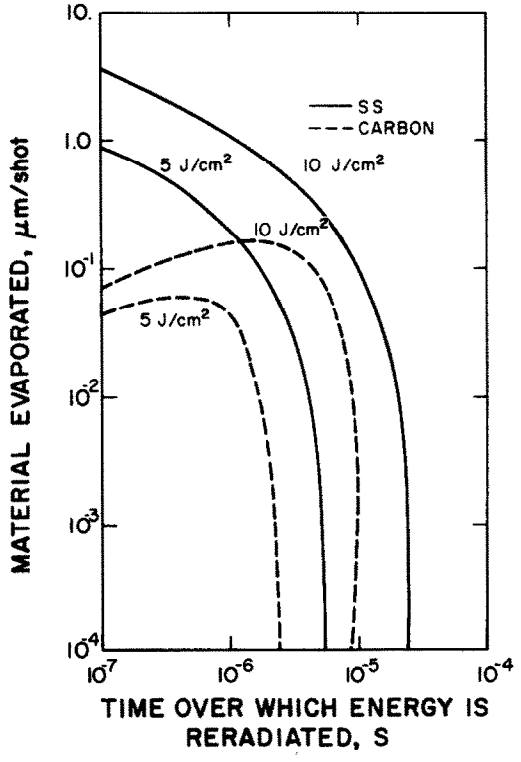

Figure 3. The evaporation of carbon and stainless steel as a function of the gas reradiation time and energy fluence.

As shown in Figure 3, the evaporation of stainless steel decreases monotonically as the reradiation time increases since more time is available for conduction into the material. Heat conduction is more sluggish in carbon, and an increase in the pulse width may increase the time available for evaporation without a significant decrease in the surface temperature. The result is that for the shorter radiation times shown in Figure 3, the evaporation of carbon increases as the pulse width increases. As the pulse width continues to increase, conduction again becomes the dominant surface cooling mechanism and the evaporation decreases monotonically. In this paper, the vapor species is assumed to be monatomic carbon, which may slightly underestimate the evaporated thickness. This is because at high temperature the dominant vapor species is C_3 rather than monatomic carbon [4]. For a reradiated energy fluence of 1 J/cm^2, the evaporated thickness was found to be less than one angstrom per shot for both carbon and stainless steel.

Figure 4 shows the melt zone thickness of stainless steel as a function of the reradiation time of the gas. For the smaller reradiation times shown, a larger melt thickness is obtained for 5 J/cm^2 than 10 J/cm^2 because evaporative erosion of the melt thickness is larger for an energy fluence of 10 J/cm^2. As the reradiation time increases, the thickness of the melt layer passes through a maximum and is larger for larger input energies. It then decreases as conduction becomes effective at larger times. The melt depth from X-ray energy deposition depends on the energy density as well as the energy spectrum. For soft X-rays, which can be modeled as a surface heat flux, Figure 4 would predict a melt depth of less than 2 microns at 10 nsec pulse duration.

3. THE DEPENDENCE OF FIRST WALL EVAPORATION ON CAVITY GAS DENSITY

A specific reactor geometry, target X-ray and debris spectrum, and buffer gas have been chosen to illustrate how the cavity gas density affects first wall evaporation. A spherical reactor cavity with a 4 meter radius was assumed. The cavity was assumed to be filled with an argon buffer gas that contains 0.2 atom percent sodium. This buffer gas was chosen because it has been used in other ICF reactor studies [8]. The target was assumed to emit 15 MJ of X-ray energy in 10 nanoseconds. The energy spectrum of the target X-rays corresponds to that of a 0.3 keV blackbody. The target debris was assumed to consist of one gram of iron expanding into the buffer gas with 15 MJ of kinetic energy (15 keV/iron ion).

In the examples that follow, the FIRE code [9] was used to compute the deposition of target X-rays and debris in the gas, as well as the subsequent radiation hydrodynamic response. The equation of state and reradiation properties of the gas that were used by FIRE were computed

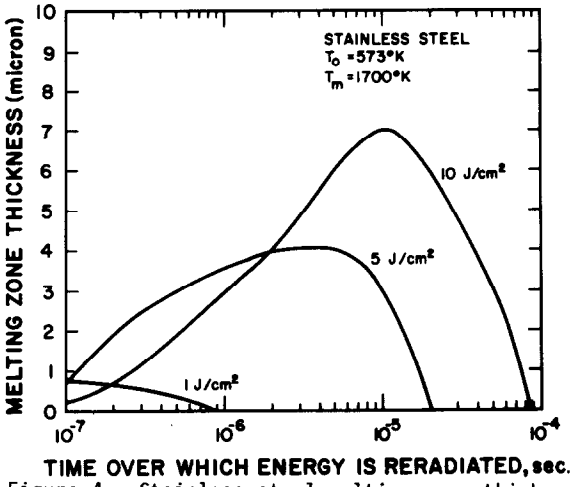

Figure 4. Stainless steel melting zone thickness as a function of reradiation time for different input energy densities.

with the MIXER code [10]. The reradiation heat flux from the gas and the spectrum of the unattenuated target X-rays were input into the A*THERMAL code to study the first wall thermal response. The flux and fluence of energy from unattenuated X-rays and gas reradiation are shown in Table 1. The argon gas densities examined correspond to 0.05, 0.5, and 5.0 torr (0°C). Although the average gas reradiation heat flux is listed in Table 1, the detailed reradiation flux history from the FIRE code was used in computing the results that follow.

Figure 5 shows the thermal response of a stainless steel first wall for the three gas densities considered in this study. The delay before the temperature rises above the ambient temperature (T_o = 573°K) is the time for the X-rays to reach the wall after the target burn. For the two lower cavity gas densities, the first wall temperature increase from X-rays is limited mainly by evaporative cooling. More unattenuated target X-rays reach the wall for the lower cavity gas densities, and consequently the lower cavity gas densities result in a higher temperature pulse from X-rays. The very high surface temperatures from X-rays at low gas pressure will actually change the surface into an ionized plasma. A lower gas density also implies a shorter reradiation pulse width, and that too will produce higher first wall temperatures. With a gas density corresponding to 0.5 torr (0°C), the temperature cools to below the melting temperature (T_m = 1700°K) before the gas reradiation induces another temperature rise. In the case of 0.05 torr, the gas reradiation keeps the surface from solidifying until about 20 μsec. A gas density corresponding to 5.0 torr keeps the surface temperature far below the melting temperature for both the X-ray pulse and the reradiation heat flux.

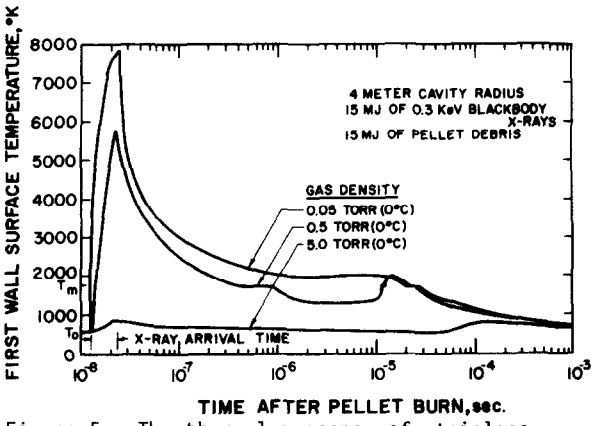

Figure 5. The thermal response of stainless steel for Ar(0.2% Na) gas densities of 0.05, 0.5, and 5.0 torr (0°C).

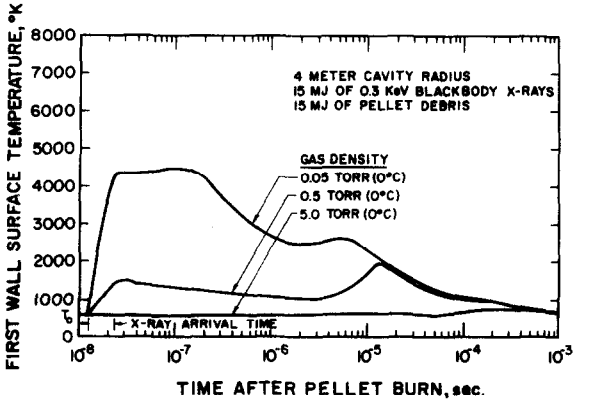

Figure 6. The thermal response of carbon for Ar (0.2% Na) gas densities of 0.05, 0.5, and 5.0 torr (0°C).

Figure 6 shows the thermal response of a carbon first wall subject to the same target X-rays and gas reradiation. The lower X-ray absorption cross section of carbon keeps the temperature rise from X-rays below that computed for stainless steel. In addition, the lower thermal conductivity of carbon prevents the temperature from dropping rapidly after the X-ray pulse. In carbon, heat conduction is sluggish enough that with a gas density corresponding to 0.05 torr, the gas reradiation continues to drive the surface temperature up slightly after the X-ray deposition. With a gas density corresponding to 5.0 torr (0°C), the temperature rise from X-rays and gas reradiation never exceeds 20°C.

Figure 7 compares the evaporation of a carbon and stainless steel first wall as a function of the cavity gas density. For the target, buffer gas, and reactor geometry chosen in this study,

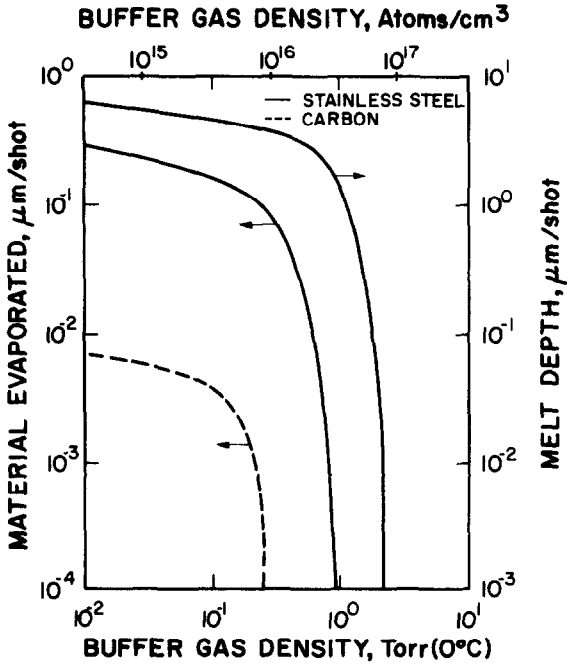

Figure 7. First wall evaporation of carbon and stainless steel vs. cavity gas density for conditions outlined in Table 1.

the evaporative erosion will not limit the lifetime of a carbon first wall unless the gas density is less than 0.3 torr (0°C). For a permanent stainless steel first wall in a commercial ICF reactor, the gas pressure should be above 0.9 torr (0°C) to avoid excessive erosion. The maximum melt depth of stainless steel is also shown in the figure (a melt depth curve for carbon is not shown because of carbon sublimation). If the cavity gas density is much below 10^{-2} torr (0°C), sputtering by debris ions begins to enhance the erosion rate.

4. CONCLUSIONS

The parametric study of first wall evaporation from X-rays shows that the lower X-ray attenuation coefficient of carbon gives it an advantage over stainless steel as a permanent first wall material. It is also shown that softer X-rays have a greater tendency to induce evaporation than hard X-rays.

The parametric study of first wall evaporation from gas reradiation shows that the low vapor pressure of carbon causes it to have a lower evaporative erosion rate than stainless steel. Also, it was observed that the evaporative erosion of carbon could increase as the time

Table 1. The Fluence and Flux of Gas Reradiation and Unattenuated Pellet X-Rays at the First Wall

Ar (0.2% Na)	Unattenuated X-Rays		Gas Reradiation	
Gas Density, Torr (0°C)	Energy Fluence, J/cm^2	Average Flux, W/cm^2	Energy Fluence, J/cm^2	Average Flux, W/cm^2
0.05	5.66	6.55×10^8	8.5	8.5×10^5
0.5	2.33	2.33×10^8	12	2.4×10^5
5.0	0.15	0.15×10^8	14	1.4×10^5

over which energy is reradiated by the gas increases if heat conduction is too sluggish. This phenomenon was not observed for stainless steel because of its relatively higher thermal conductivity.

The evaporation from unattenuated X-rays and gas reradiation has been computed for various buffer gas densities. This is done for a specific reactor geometry, target X-ray and debris spectra, and type of buffer gas. The results show that for the parameters specified in this study, the evaporative erosion of stainless steel falls to a negligible value as the ambient buffer gas density is increased to about 1 torr (0°C). The evaporative erosion of carbon is negligible if the ambient gas density is greater than about 0.3 torr (0°C). Below these densities, the evaporation will keep a carbon or stainless steel first wall from lasting the life of a commercial ICF plant.

ACKNOWLEDGMENT

The authors would like to acknowledge the partial support of this research from the Kernforschungszentrum Karlsruhe of the Federal Republic of Germany and Sandia Laboratory, Albuquerque, NM.

REFERENCES

[1] McCarville, T.J., Hassanein, A.M., Kulcinski, G.L., The response of stainless steel to the pellet debris in a laser fusion reactor, presented at the 5th International Conference on Structural Mechanics in Reactor Technology, Berlin, Germany, Vol. N, August 1979.

[2] Conn, R.W., et al., SOLASE - a conceptual laser fusion reactor design, University of Wisconsin Fusion Engineering Program Report UWFDM-220, December 1977.

[3] Hassanein, A.M., Kulcinski, G.L., A*THERMAL code description, University of Wisconsin Fusion Engineering Program Report, to be published.

[4] Hassanein, A.M., Kulcinski, G.L., Wolfer, W.G., Vaporization and melting of materials in fusion devices, presented at the Second Topical Meeting on Fusion Reactor Materials, Seattle, WA, August 1981.

[5] Choong, S. Kim, Thermophysical properties of stainless steel, ANL-75-55, Argonne National Laboratory, Sept. 1975.

[6] Rasor, N.S., McClelland, J.D., Thermal properties of graphite, molybdenum and tantalum to their destruction temperatures, J. Phys. Chem. Solids 15 (1959) 17-26.

[7] Biggs, F., Lighthill, R., Analytical approximations for total and energy absorption cross sections for photon-atom scattering, SC-PR-720685, Sandia Laboratories, Albuquerque, NM, December 1972.

[8] Peterson, R.R., Cooper, G.W., Moses, G.A., Cavity gas analysis for light ion beam fusion reactors, Nucl. Tech./Fusion (July 1981).

[9] Moses, G.A., McCarville, T.J., Peterson, R.R., Improvements in the FIRE code for simulating the response of a cavity gas to inertial confinement fusion target explosions, University of Wisconsin Fusion Engineering Program Report UWFDM-407, 1981.

[10] Peterson, R.R., Moses, G.A., MIXER - a multi-series optical data and equation of state computer code, University of Wisconsin Fusion Engineering Program Report UWFDM-372, September 1980.